JOURNAL OF SOLID STATE CHEMISTRY 114, 199–205 (1995)

Structural and Magnetic Studies of $Bi_2Fe_{4-x}Al_xO_9$

D. M. Giaquinta,* G. C. Papaefthymiou,† and H.-C. zur Loye*,[1]

*Department of Chemistry, and †the Francis Bitter National Magnet Laboratory, Massachusetts Institute of Technology, Cambridge, Massachusetts 02139

Received February 28, 1994; in revised form May 10, 1994; accepted May 19, 1994

The solid solution $Bi_2Fe_{4-x}Al_xO_9$ ($0 \leq x \leq 4$) was synthesized and investigated by powder X ray diffraction, Mössbauer spectroscopy, and magnetic susceptibility measurements. The structure of the $x = 2$ member was refined using the Rietveld method. The structure is orthorhombic with space group *Pbam* (No. 55), $a = 7.8611(3)$ Å, $b = 8.2753(3)$ Å, $c = 5.8535(3)$ Å. The aluminum in the structure substitutes in both available coordination geometries, octahedral and tetrahedral, with equal probability. Magnetic susceptibility and Mössbauer measurements of the materials with $x \leq 1$ display antiferromagnetic behavior. The Néel temperature, T_N, exhibits a strong dependence on x, decreasing rapidly with aluminum doping. Spin-glass-like behavior is also observed for values of $x \geq 0.6$.

INTRODUCTION

The tailoring of advanced materials often relies on the ability to substitute a particular element directly into a specific crystallographic site. On theoretical grounds, coordination preferences may be generalized as resulting from size, oxidation state, and electronegativity of the substituent element. In practice, however, the chemistry of site-specific substitution remains, to this date, largely experimental in nature. In compounds with several inequivalent cation coordination sites, substitution experiments afford the only means for ascertaining which elements may be inserted into a certain site. We have previously reported structural, magnetic and Mössbauer studies of one such system, the solid solution $Bi_2Fe_{4-x}M_xO_{9+\delta}$, where M = Ga and Mn (1, 2).

The $Bi_2M_4O_{9+\delta}$ structure contains nonmagnetic planes of bismuth oxide that sandwich a magnetic transition metal oxide region consisting of two types of metal coordination sites, tetrahedral and octahedral (3–5) (Fig. 1). The chemistry of this structure type, $Bi_2M_4O_{9+\delta}$, is of special interest as an example of site-specific substitution in a layered material containing both octahedral and tetrahedral cation coordination geometries. In this paper we report additional studies on the $Bi_2M_4O_{9+\delta}$ system, specifically, structural, magnetic susceptibility, and Mössbauer spectroscopic investigations of the solid solution $Bi_2Fe_{4-x}Al_xO_9$ for $0 \leq x \leq 4$. The aim of this investigation was: (a) to elucidate how the magnetically coupled octahedral and tetrahedral sites affect the complex magnetic behavior of this system, and (b) to ascertain whether its magnetic properties can be systematically altered by elemental substitutions. Structure–property relationships of the transition metal oxide region and the ensuing magnetism of the $Bi_2Fe_4O_9$-based system were investigated by substituting the diamagnetic ion, Al^{3+}, for the magnetic ion, Fe^{3+}. In the previously studied system, $Bi_2Fe_{4-x}Ga_xO_9$, the cation site specificity of gallium for tetrahedral substitution was only 60% (1). Nonetheless, interesting magnetic interactions were observed as the doping of diamagnetic gallium for iron caused spin frustration and spin-glass-like behavior. The present study of the solid solution $Bi_2Fe_{4-x}Al_xO_9$ was pursued to compare the properties and substitution chemistry of aluminum, gallium, and iron.

[1]To whom correspondence should be addressed.

EXPERIMENTAL SECTION

Sample Preparation

Polycrystalline samples of the solid solution $Bi_2Fe_{4-x}Al_xO_9$ were prepared in increments of $x = 0.25$ for the range of $0 \leq x \leq 1$ and in increments of 1 for values of $1 \leq x \leq 4$. Stoichiometric amounts of the oxides Bi_2O_3 (Cerac, 99.9%), Fe_2O_3 (Cerac, 99.99%), and Al_2O_3 (AESAR, 99.99%), were ground under acetone, pressed into pellets, and heated at 850°C in air for two weeks with frequent grindings. The pellets were heated in Al_2O_3 crucibles on platinum foil to prevent aluminum contamination.

Structural Characterization

Polycrystalline samples were structurally characterized by powder X ray diffraction on a Rigaku RU300 at 10 kW with CuK_α radiation ($\lambda = 1.54184$ Å). NBS mica (SRM 675) was used as a standard for accurate peak positions. A polycrystalline sample of $Bi_2Fe_2Al_2O_9$ was used

0022-4596/95 $6.00

for the structure refinement. An X ray powder diffraction step scan was collected from 5°–120° 2Θ, using a step size of 0.02° 2Θ and a time of 5 sec/step. A Rietveld refinement of the powder X ray diffraction data was performed using refinement package GSAS (6). The single crystal structure of $Bi_2Fe_2Ga_2O_9$(1) was used as the starting model.

Magnetic Measurements

Magnetic data were collected on sintered pieces using a Quantum Design SQUID magnetometer at temperatures ranging from 5 to 400 K and in applied fields ranging from 5 to 40 kG. A scan length of 6 cm was used and 20 measurements were performed over the scan length. A total of 3 scans were averaged for each data point. All data were corrected for the diamagnetic contribution of the Kel-F sample holder.

Mössbauer Spectroscopy

Mössbauer spectra of various aluminum doping levels between $0 \leq x \leq 2$ were obtained using a conventional constant acceleration spectrometer. Sample temperatures in the range $20 \leq T \leq 300$ K were achieved by the use of a Janis Supervaritemp dewar and a Lake Shore temperature controller. The source was ^{57}Co(Rh) maintained at room temperature. Isomer shifts are reported relative to metallic iron at room temperature.

RESULTS

Structural

The structure of $Bi_2Fe_2Al_2O_9$ is shown in Fig. 1. Structure determination parameters are shown in Table 1. The final positional and thermal parameters are listed in Table 2 and selected interatomic bond distances are shown in Table 3. The structure of $Bi_2Fe_2Al_2O_9$ consists of columns of edge-sharing octahedra which are corner-shared with corner-sharing tetrahedra as shown in Fig. 2. The octahedra are located in layers perpendicular to the c axis that are separated by doubly packed tetrahedral layers. These layers form slabs of alternating octahedral–tetrahedral–octahedral coordination. The slabs in turn are separated from each other by planes of bismuth and oxygen (see Fig. 1). The octahedra are connected across the tetrahedral and bismuth oxide layer *via* edge-sharing oxygens

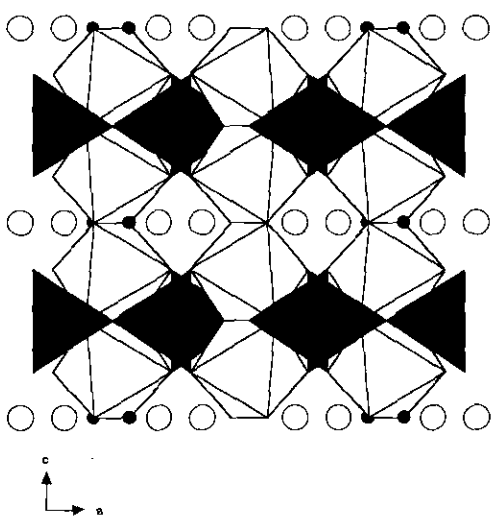

FIG. 1. Polyhedral representation of the octahedral and tetrahedral cation coordination geometries of $Bi_2Fe_2Al_2O_9$. Oxygen atoms are located at the apices of each polyhedron. ○ = Bismuth, ● = oxygen.

TABLE 1
Crystal Structure Determination Parameters

Empirical formula	$Bi_2Fe_2Al_2O_9$				
Formula weight (g/mol)	727.61				
Crystal system	orthorhombic				
Space group	*Pbam* (No. 55)				
Lattice parameters (Å)					
a	7.8611 (3)				
b	8.2753 (3)				
c	5.8535 (3)				
Volume (Å^3)	380.80				
Z	2				
Diffractometer	Rigaku RU300				
Radiation	Cu$K\alpha$ (λ = 1.54184 Å)				
Temperature (°C)	24				
2Θ range	$10 \leq 2\Theta \leq 100$				
Number of observations	4250				
Refinement	Rietveld technique; program GSAS[a]				
Peak shape function	pseudo-Voigt[b]				
Peak shape coefficients					
GU	1.675 E + 3	GV	−5.292 E + 2	GW	1.106 E + 2
LX	3.669 E + 0	LY	3.951 E + 1	stec	2.633 E + 0
ptec	−1.094 E − 1				
Background	10 coefficient cosine Fourier series				
Residuals: *Rwp*, *Rp*	0.0944, 0.0671				

[a] GSAS: General Structure Analysis System, LANSCE, Los Alamos National Laboratory
[b] *J. Appl. Cryst.* **15**, 615–620 (1982).

TABLE 2
Atomic Coordinates for $Bi_2Fe_2Al_2O_9$

Atom	*x*	*y*	*z*	U_{iso}
Bi	0.1736(1)	0.1713(1)	0	0.015
Al(1)	½	0	0.2594(8)	0.019
Al(2)	0.3550(6)	0.3414(6)	½	0.007
Fe(1)	0.3550(6)	0.3414(6)	½	0.019
Fe(2)	½	0	0.2594(8)	0.007
O(1)	0	0	½	0.012
O(2)	0.3699(9)	0.215(1)	0.238(1)	0.005
O(3)	0.134(2)	0.408(2)	½	0.004
O(4)	0.148(2)	0.435(2)	0	0.016

TABLE 3
Selected Bond Lengths (Å) and Bond Angles(°)

Bi–O(2)	2.110(7) × 2	O(2)–Bi–O(2)	82.7(4)
Bi–O(2)	2.921(7) × 2	O(2)–Bi–O(4)	84.2(4) × 2
Bi–O(4)	2.187(14)	O(2)–Bi–O(4)	73.3(3) × 2
Bi–O(4)	2.410(13)	O(4)–Bi–O(4)	149.7(2)
Bi–oct.	3.301(2) × 4	O(2)–oct.–O(2)	173.1(5)
Bi–oct.	3.401(2) × 2	O(2)–oct.–O(3)	96.7(4)
oct.–O(2)	2.054(8) × 2	O(2)–oct.–O(3)	88.4(4)
oct.–O(3)	1.917(9) × 2	O(2)–oct.–O(4)	84.2(4)
oct.–O(4)	1.988(9) × 2	O(2)–oct.–O(4)	90.5(5)
oct.–oct.	3.036(9) × 2	O(3)–oct.–O(3)	85.4(7)
oct.–oct.	2.817(9) × 2	O(3)–oct.–O(4)	97.6(4)
tet.–O(1)	1.738(5)	O(3)–oct.–O(4)	172.3(5)
tet.–O(2)	1.861(8) × 2	O(4)–oct.–O(4)	80.4(7)
tet.–O(3)	1.823(12)	O(1)–tet.–O(2)	112.5(3)
		O(1)–tet.–O(3)	113.5(5)
		O(2)–tet.–O(2)	110.9(6)
		O(2)–tet.–O(3)	103.3(4)

Note. Oct. and tet. represent the position of the octahedral and tetrahedral cation site, respectively.

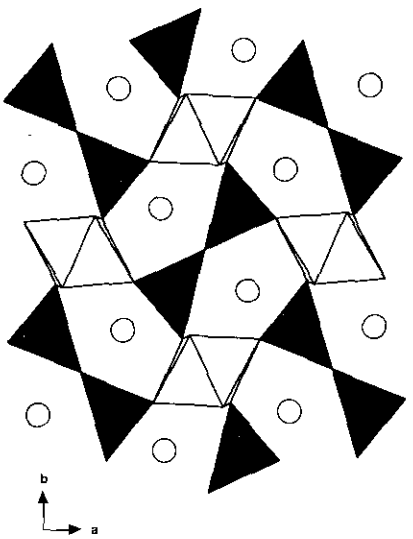

FIG. 3. Polyhedral representation of $Bi_2Fe_2Al_2O_9$ viewed perpendicular to the *ab* plane. ○ = Bismuth.

located in the tetrahedral and bismuth oxide plane, respectively. The corner-shared tetrahedra are coupled perpendicular to the octahedral chains, linking chains to each other. A view down the length of the octahedral chains is shown in Fig. 3.

The octahedral metal–oxygen bonds vary from 1.92 to 2.05 Å, with the shortest octahedral metal–oxygen distance, 1.92 Å, being an edge-sharing distance within the octahedral chains. The metal–oxygen bond lengths in the slightly distorted tetrahedra vary from 1.74 to 1.86 Å, as shown in Table 2. The shortest metal–oxygen bond length in the tetrahedra, 1.74 Å, corner-shares two adjacent tetrahedra. All oxygens in the structure are tetrahedrally coordinated.

The iron and aluminum atoms are statistically distributed over the octahedral and tetrahedral sites, in contrast with the solid solution $Bi_2Fe_{4-x}Ga_xO_9$, where the gallium sits preferentially on the tetrahedral sites in a ratio of 3 : 2(1). The powder pattern of $Bi_2Fe_2Al_2O_9$ is shown in Fig. 4 and *hkl* values are listed in Table 4. Lattice parameters for all members of the solid solution were also determined from powder X ray diffraction patterns. The lattice parameters were found to follow Vegard's law (7) across the range of x. The compounds gradually changed color across the solid solution from $Bi_2Fe_4O_9$, orange-brown, to $Bi_2Al_4O_9$, pale yellow.

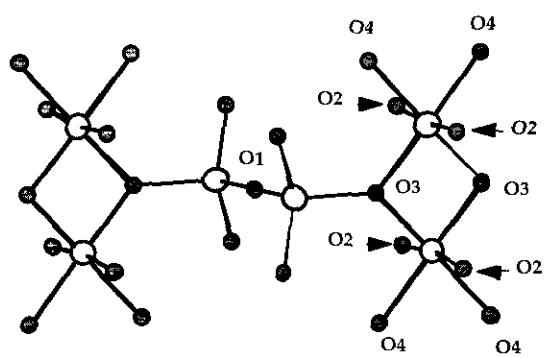

FIG. 2. View of the local symmetry surrounding the tetrahedral and the octahedral cation coordination sites.

Magnetic Susceptibility

Magnetic measurements showed that the solid solution $Bi_2Fe_{4-x}Al_xO_9$, for $0 \leq x \leq 1$ orders antiferromagnetically. This is in agreement with the previously reported antiferromagnetic behavior of $Bi_2Fe_4O_9$ (4) and that of our solid solution $Bi_2Fe_{4-x}Ga_xO_9$ (1). The susceptibility plots display broad maxima, as shown in Fig. 5, but not as broad as those seen in either the undoped $Bi_2Fe_4O_9$ system or the solid solution $Bi_2Fe_{4-x}Ga_xO_9$ (1). Broadness of susceptibility maxima is often associated with either lower dimensional magnetic ordering (8) or a second-order 3-dimensional magnetic phase transition (9). The presence of uncompensated spins is seen as a rise in magnetic susceptibility at low temperatures in the susceptibility *vs* temperature plot of the $x = 0.25$ compound.

The change in T_N with aluminum doping in $Bi_2Fe_{4-x}Al_xO_9$ is shown in Fig. 6. The Néel temperature, T_N, was determined as the temperature of the point of inflection below the maximum (9). The behavior is similar to what we reported on the $Bi_2Fe_{4-x}Ga_xO_9$ solid solution (1). Low levels of Al doping, up to $x = 0.25$, cause very little change in T_N. Although the presence of diamagnetic alu-

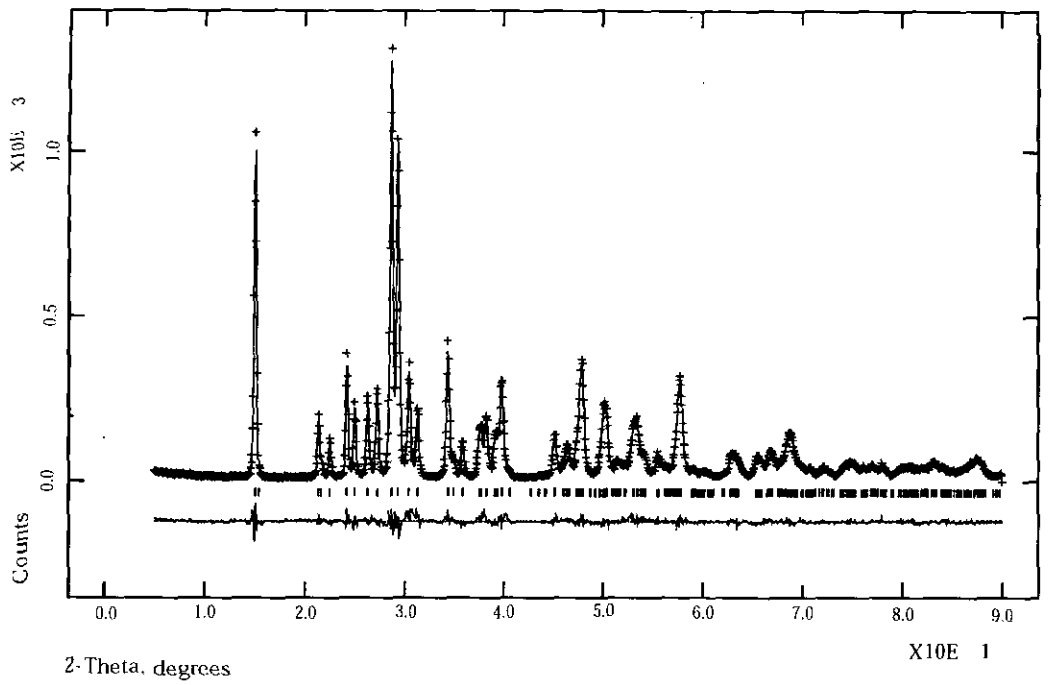

FIG. 4. The observed, calculated, and difference profiles of the powder X ray diffraction Rietveld refinement of $Bi_2Fe_2Al_2O_9$.

minum must cause some disruption in the network of superexchange interactions between the iron atoms, the ordering temperature is affected only slightly for such low dopant levels. When the exchange interactions are sufficiently disrupted the ordering temperature drops from 240 to 25 K for $x = 1$. Obviously for this doping

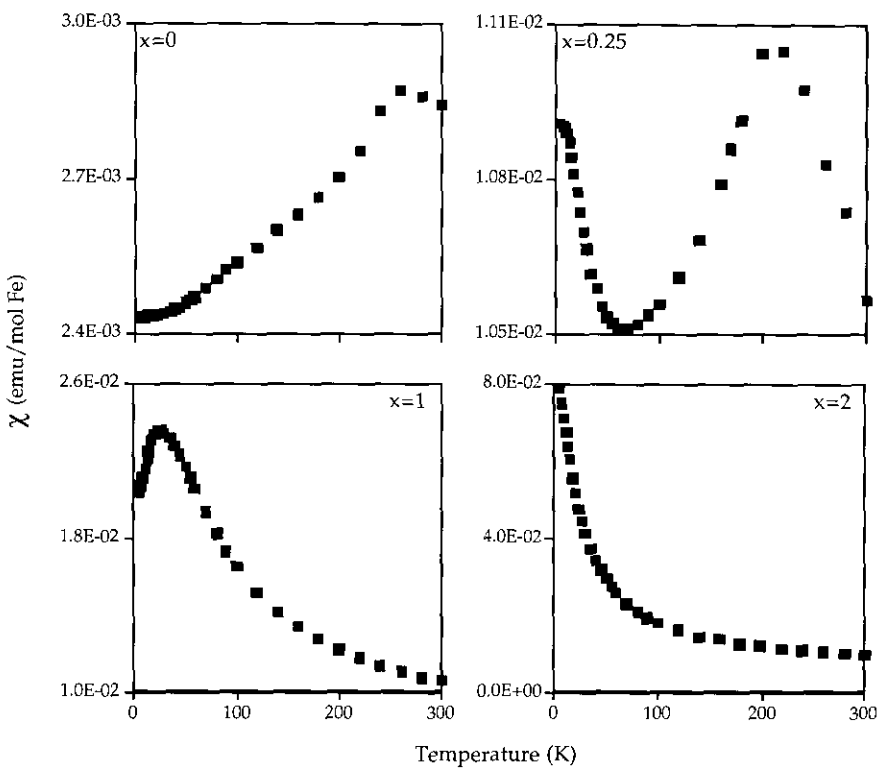

FIG. 5. Susceptibility vs temperature plots for several values of x for the solid solution $Bi_2Fe_{4-x}Al_xO_9$.

TABLE 4
hkl values for Fig. 4[a]

d_{calc} (Å)	h	k	l	I_{calc}	I_{obs}
5.853	0	0	1	79	82
4.138	0	2	0	13	15
4.083	1	1	1	3	5
3.931	2	0	0	10	11
3.661	1	2	0	26	29
3.550	2	1	0	17	17
3.379	0	2	1	19	19
3.263	2	0	1	25	22
3.104	1	2	1	100	100
3.036	2	1	1	85	82
2.9267	0	0	2	28	26
2.8497	2	2	0	16	17
2.6035	1	1	2	33	32
2.5622	2	2	1	3	3
2.4981	3	1	0	11	9
2.3894	2	2	9	13	
2.3475	2	0	2	17	15
2.2976	3	1	1	7	10
2.2583	2	1	2	27	24
2.0007	1	4	0	11	10
1.9450	1	3	2	4	6
1.9121	4	1	0	7	7
1.8932	1	4	1	21	25
1.8176	4	1	1	16	15
1.7249	1	2	3	12	9
1.7100	2	1	3	12	11
1.6517	1	4	2	7	4
1.6008	4	1	2	10	14
1.5935	3	3	2	24	22
1.4761	2	5	1	5	5
1.4634	0	0	4	5	5
1.4255	5	2	1	4	4
1.3993	3	5	0	2	4
1.3657	4	1	3	4	6
1.3589	1	2	4	2	3
1.1151	1	2	5	2	3

[a] Calculated peaks which were unobserved in the powder pattern are not included.

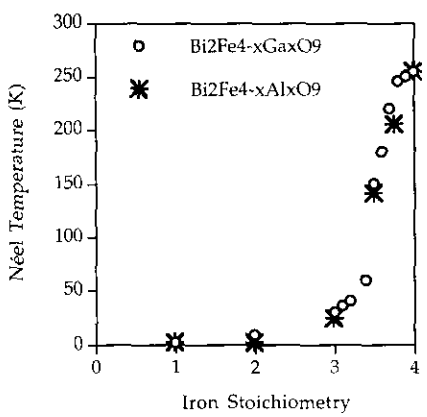

FIG. 6. Néel temperature vs iron stoichiometry for the solid solution $Bi_2Fe_{4-x}Al_xO_9$. Values are compared with those of $Bi_2Fe_{4-x}Ga_xO_9$ (1).

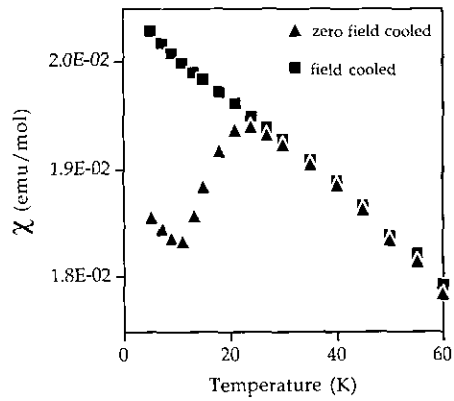

FIG. 7. Magnetic field history dependence of $Bi_2Fe_3AlO_9$ cooled in the presence or absence of an external magnetic field.

level, the interaction network critical for the high antiferromagnetic phase transition temperature is destroyed. Additional doping causes the transition temperature to decrease gradually toward zero.

The susceptibility below the antiferromagnetic ordering temperature shows field history dependence as shown in Fig. 7. Placing a sample into the magnetometer with the applied field on results in magnetic behavior that is ferrimagnetic in appearance, while placing a sample into the magnetometer with the magnetic field off produces behavior that is characteristic of an antiferromagnet. No field history dependent behavior was observed for samples with $2 \leq x \leq 4$ as zero-field-cooled and field-cooled samples exhibited identical paramagnetic susceptibility curves.

Mössbauer Spectroscopy

Mössbauer spectra for $0 \leq x \leq 2$ were collected at selected temperatures between room temperature and 20 K. Representative spectra for $Bi_2Fe_{3.5}Al_{0.5}O_9$ are shown in Fig. 8. Mössbauer parameters derived from least-square fits of the experimental data to theoretical models, assuming axial electric field gradients ($\eta = 0$), are tabulated in Table 5.

At high temperatures ($T = 200$ K) the spectrum of $Bi_2Fe_{3.5}Al_{0.5}O_9$ is paramagnetic and composed of the superposition of two quadrupole doublets with isomer shifts and quadrupole splittings $\delta_1 = 0.46$ mm/sec and $\Delta E_{Q_1} = 0.56$ mm/sec, and $\delta_2 = 0.21$ mm/sec, and $\Delta E_{Q_2} = 0.85$ mm/sec consistent with high spin Fe^{+3} ions in octahedral and tetrahedral environments, respectively (10). The integrated intensity ratio of the two signals is 49 : 51 in accordance with the crystallographic structure of the compound which contains equal numbers of tetrahedral and octahedral sites.

The onset of magnetic hyperfine splitting in the Mössbauer spectra for $x = 0.5$ occurs at $T_N \sim 140$ K, in agree-

ment with our magnetic susceptibility measurements. With decreasing temperature, the magnetic hyperfine splitting increases as the magnetization of the compound approaches saturation. (See Table 5.) Two magnetic subcomponents, associated with the octahedral and tetrahedral iron sites, were resolved. There is a slight difference in local magnetic moments between the two subsites that is reflected in a difference of the magnetic hyperfine fields, for example, H_{hf}(oct) = 474 kOe and H_{hf}(tet) = 434 kOe at T = 50 K. (See Table 5). The overall magnetic behavior is similar to that of the $Bi_2Fe_{4-x}Ga_xO_9$ solid solution (1) and is consistent with 3-dimensional magnetic ordering. The anomalous spectral broadening indicative of a spin rearrangement phase transition in the Mössbauer spectra of $Bi_2Fe_4O_9$ was not observed in the spectra of the $Bi_2Fe_{4-x}Al_xO_9$ solid solution (1).

The Mössbauer spectra of $Bi_2Fe_{4-x}Ga_xO_9$ that were examined for the range of $0 \leq x \leq 1$ showed temperature behavior consistent with 3-dimensional magnetic ordering with T_N decreasing with increasing x. As was the case for the gallium-doped system (1), we observed that the experimental H_{hf} data followed a smooth Brillouin-like functional temperature dependence as expected for a 3-D magnetic phase transition described by molecular field theory (9, 11) (Fig. 9).

DISCUSSION

Structurally, the $Bi_2Fe_{4-x}Al_xO_9$ solid solution is similar to the previously reported $Bi_2Fe_{4-x}Ga_xO_9$ solid solution (1). The lattice parameters are slightly smaller in the aluminum compound due to that the radius of Al^{+3} (0.54 Å) is smaller than that of Ga^{+3} (0.62 Å). Lattice parameters change in a linear fashion across the solid solution in the manner described by Vegard's Law (7). This is to be expected since according to both diffraction and Mössbauer data, the iron and aluminum atoms are randomly distributed on the octahedral and tetrahedral coordination sites, unlike $Bi_2Fe_{4-x}Ga_xO_9$, where the gallium had a 3 : 2 preference for the tetrahedral site. This slight struc-

TABLE 5
Mössbauer Parameters for the Solid Solution $Bi_2Fe_{4-x}Al_xO_9$

x	T (K)	δ[a] (mm/sec)	ΔE_Q or ε[b] (mm/sec)	H_{hf} (kOe)	$\Gamma/2$ (mm/sec)	Percentage of Area (%)	T_N (K)
0.0	250	0.48[c]	0.54	—	0.15	48	245
		0.19[d]	0.78	—	0.15	52	
	230	0.34[e]	0.225	277	0.27	100	
	200	0.38[e]	0.18	358	0.95	100	
	150	0.45[c]	0.15	432	0.14	42	
		0.34[d]	0.16	412	0.18	58	
	4.2	0.48[c]	0.15	505	0.16	50	
		0.34[d]	0.16	467	0.17	50	
0.5	200	0.46[c]	0.56	—	0.18	49	140
		0.21[d]	0.85	—	0.18	51	
	120	0.45[c]	0.14	366	0.30	57	
		0.34[d]	0.06	311	0.30	43	
	80	0.46[c]	0.14	439	0.28	58	
		0.38[d]	0.06	389	0.28	42	
	50	0.46[c]	0.14	475	0.22	46	
		0.38[d]	0.06	434	0.22	54	
1.0	200	0.48[c]	0.60	—	0.18	47	25
		0.21[d]	0.83	—	0.18	53	
	20	0.43[c]	0.14	455	0.30	48	
		0.34[d]	0.06	400	0.30	52	
2.0	200	0.47[c]	0.64		0.19	50	
		0.21[d]	0.88		0.17	50	

[a] Isomer shifts are reported relative to metallic iron at room temperature.

[b] For magnetically split spectra, $\varepsilon = (\frac{1}{4})\Delta E_Q(3\cos^2\theta - 1)$, where θ is the angle between the magnetic hyperfine field, H_{hf}, and the principal component of the electric field gradient at the site of the nucleus (10).

[c] Octahedral sites.

[d] Tetrahedral sites.

[e] Single, averaged site fits due to unresolved octahedral and tetrahedral subsites from Giaquinta *et al.* (1).

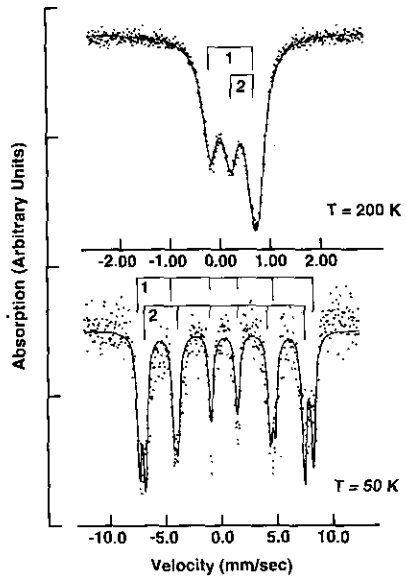

FIG. 8. Mössbauer spectra of $Bi_2Fe_{3.5}Al_{0.5}O_9$. Top, paramagnetic spectrum observed at $T = 200$ K. Bottom, magnetically ordered spectrum recorded at $T = 50$ K. Note the change in velocity scale. Spectral components 1 and 2 are associated with octahedral and tetrahedral subsites, respectively.

tural difference is characteristic of the crystal chemistry differences between aluminum and gallium and not likely due to the smaller radius of aluminum (12, 13). For instance, in their respective binary oxides, the coordination of Al^{+3} is octahedral while that of Ga^{+3} is tetrahedral.

Rapid drops in the antiferromagnetic phase transition temperature for doping levels exceeding some small threshold level are characteristic of systems having competing magnetic interactions (14) and have been observed in other iron containing compounds (15). In the presence of competing magnetic interactions, the magnetic order of the undoped system breaks down rapidly with spin dilution and spin-glass phenomena can occur. The magnetic trends seen in both the $Bi_2Fe_{4-x}Al_xO_9$ and the $Bi_2Fe_{4-x}Ga_xO_9$ solid solutions are consistent with this behavior. The disruption of magnetic order in both systems beyond a threshold dopant level is most likely the result of a spin frustration phenomenon due to competing exchange interactions. The effects of the spin frustration may be seen both in the uncompensated spin region of the $x = 0.25$ compound in Fig. 5 and in the magnetic field history of the $x = 1$ compound shown in Fig. 7.

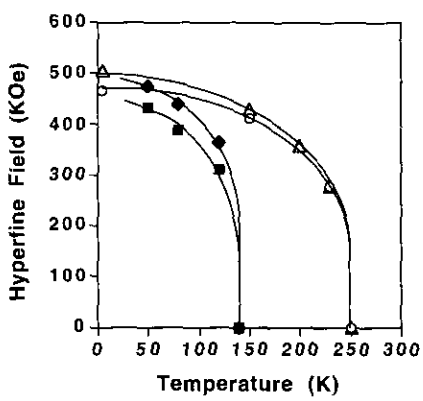

FIG. 9. Temperature dependence of the observed magnetic hyperfine fields at octahedral (◆) and tetrahedral (■) iron subsites for $Bi_2Fe_{3.5}Al_{0.5}O_9$. Values are compared with those of the octahedral (△) and tetrahedral (○) iron subsites of $Bi_2Fe_4O_9$. The solid lines are drawn through the points to aid the eye.

CONCLUSIONS

The solid solution $Bi_2Fe_{4-x}Al_xO_9$ has been investigated structurally and magnetically, using X ray powder diffraction, magnetic susceptibility, and Mössbauer spectroscopy. A statistical distribution of aluminum and iron over the octahedral and tetrahedral cation coordination sites was observed. The magnetic ordering behavior, as seen by susceptibility and Mössbauer measurements, is 3-dimensional in nature, with the ordering temperature dropping rapidly with increasing aluminum doping. This behavior is consistent with the disruption of several competing magnetic exchange interactions and qualitatively analogous with what we reported previously for $Bi_2Fe_{4-x}Ga_xO_9$.

ACKNOWLEDGMENT

This work was supported by the Massachusetts Institute of Technology, Center for Materials Science and Engineering, Grant DMR9022933.

REFERENCES

1. D. Giaquinta, H.-C. zur Loye, G. C. Papaefthymiou, and W. M. Davis, *J. Solid State Chem.* **99,** 120 (1992).
2. D. Giaquinta and H.-C. zur Loye, *J. Alloys Comp.* **184,** 151 (1992).
3. N. Shamir, E. Gurewitz, and H. Shaked, *Acta Crystallogr. Sect. A* **34,** 662 (1978).
4. N. Niizeki and M. Wachi, *Z. Kristallogr.* **127,** 173 (1968).
5. A. G. Tutov, I. E. Myl'nikova, N. N. Parfenova, V. A. Bokov, and S. A. Kizhaev, *Sov. Phys. Solid State* **6,** 963 (1964).
6. A. C. Larson and R. B. von Dreele, GSAS, General Structure Analysis System, Los Alamos National Laboratory, Los Alamos, NM, 1990.
7. A. R. West, "*Solid State Chemistry and Its Applications.*" Wiley, New York, 1984.
8. R. L. Carlin, "*Magnetochemistry.*" Springer-Verlag, Berlin, 1986.
9. M. E. Fisher, *Philos. Mag.* **7,** 1731 (1962).
10. N. N. Greenwood and T. C. Gibb, "*Mössbauer Spectroscopy.*" Chapman and Hall, London, 1971.
11. L. J. deJongh and A. R. Miedema, *Adv. Phys.* **23,** 1 (1974).
12. M. Marezio, J. P. Remeika, and P. D. Dernier, *Mater. Res. Bull.* **1,** 247 (1966).
13. H. W. Jaffe, "*Crystal Chemistry and Refractivity.*" Cambridge Univ. Press, Cambridge, 1988.
14. F. Scholl and K. Binder, *Z. Phys. B* **39,** 239 (1980).
15. J. L. Dormann and M. Nogues, *J. Phys. Condens. Matter* **2,** 1223 (1990).